Int. J. Electrochem. Sci., 8 **(2013)** 347 - 358

International Journal of
ELECTROCHEMICAL
SCIENCE
www.electrochemsci.org

Preparation and Characterization of Sandwich-Typed Three-Dimensional Nanoporous Copper-Supported Tin Thin-Film Anode for Lithium Ion Battery

Wenbo Liu[1,2,*], *Shichao Zhang*[1,*], *Ning Li*[2], *Shenshen An*[1] *and Jiwei Zheng*[1]

[1] School of Materials Science and Engineering, Beihang University, Beijing 100191, China
[2] School of Manufacturing Science and Engineering, Sichuan University, Chengdu 610065, China
[*]E-mail: liuwenbo_8338@163.com; csc@buaa.edu.cn

Received: 10 September 2012 / *Accepted:* 27 November 2012 / *Published:* 1 January 2013

To ameliorate the large volume expansion/contraction during lithiation/delithiation process of metallic tin anode for high-performance lithium-ion batteries (LIBs), a unique sandwich-typed three-dimensional nanoporous copper-supported tin (3D-NPC/Sn) thin-film anode was prepared by partly chemical dealloying of as-cast Al 50 at.% Cu alloy slices followed by electroless depositing of a thin layer of tin in an alkaline solution. The microstructure of the 3D-NPC/Sn thin-film anode was characterized using X-ray diffraction, scanning electron microscopy, energy dispersive X-ray analysis, and its electrochemical performance was investigated by galvanostatic charge/discharge cycling test. The results show that the 3D-NPC/Sn thin-film anode exhibits higher capacity and better cyclability than that of two-dimensional (2D) counterpart, which can be attributed to the special 3D porous structure and large active surface area facilitating accommodation of structural strain and acceleration of mass transportation, suggesting that the 3D-NPC/Sn thin-film anode has a promising application in high-performance LIBs.

Keywords: Lithium ion battery; Dealloying; Nanoporous; 3D structure; Tin anode

1. INTRODUCTION

Although widely used in the field of various portable electric devices as a power supply, lithium ion batteries still have attracted much attention in attempts to ameliorate the performance of their inside components. As a successful application in lithium-ion batteries, carbonaceous materials have many advantages such as stable charge-discharge properties and low-cost [1]. However, since their theoretical capacity is only 372 mAh g^{-1} for LiC_6, it is great important to develop new anode materials with higher capacity for LIBs. Compared with graphite, Sn and Li can form $Li_{4.4}Sn$ in

lithiation process with theoretical capacity of 994 mAh g^{-1}, which has attracted researchers' great interest [2]. Unfortunately, such material is known to suffer from dramatic severe volume change (expansion and contraction over 200%) during lithiation/delithiation process, which leads to pulverization and poor cycle life, and thus severely inhibited its application in LIBs [3-8].

The current strategies to overcome the pulverization of tin mainly include reducing the size of active material to nano-scale [9-11], using active/inactive composite as strain buffer [4,12-13], and adopting 3D current collector [14,15]. Nanostructured material have unique advantages in mass transport which leads to easy diffusion of electron and ion, higher electrode/electrolyte interfacial contact area and better accommodation of structural strain during lithiation/delithiation reactions [16]. Simon et al. [17] reported a nano-architectured electrode by depositing tin on copper nanopillars, which exhibits good cycle performance. Moreover, in order to alleviate the severe volume change during cycling, some researchers dispersed tin into inactive components to form the active/inactive composite system and strengthen the interfacial binding force, such as Sn-Cu, Sn-Ni, Sn-Co, Sn-Mo, Sn-C, and so forth [18-23]. Tamura's study showed that the capacity retention after 10 cycles was improved from 20% to 94% due to the formation of Cu_6Sn_5 intermetallic layers between copper and tin layers by heat treatment, which enhanced the interface strength [24]. Although two- and multi-component alloys can improve the cyclability for LIBs, they still are far from commercialization. Besides, in order to further enhance the cyclability of active materials with high theoretical capacity, 3D substrates were employed as candidates of current collectors, such as carbon paper, nickel foam, copper foam, and copper cellular architecture [16,25-28]. Compared to the compact one, the foamy metals possess several prominent advantages. Firstly, it offers a good conductive environment for active materials. Moreover, its stress absorbability is beneficial to construct a stretch electrode system, which would insure good combination between active materials and substrate so that preventing the electrode failure during cycling [29].

3D nanoporous metals (NPMs) prepared by dealloying, as novel functional materials, have recently attracted considerable interest in a wide variety of technological applications including catalysis, sensors, actuators, fuel cells, microfluidic flow controllers, and so forth [30-33]. Dealloying is a special corrosion process during which the less noble atoms is selectively dissolved from alloy, leaving behind the noble metal atoms that diffused along alloy/solution interfaces and agglomerated into the porous network [34]. In the previous work, many NPMs with uniform/complicated porous structures had been successfully fabricated through some facile approaches on a basis of understanding of physical nature of dealloying and their formation mechanisms were revealed in detail [35-54]. Though NPMs have shown many achievements, as one of the most promising application fields of NPMs, few researches have so far conducted in LIBs.

In this article, we propose a strategy to prepare a unique sandwich-typed 3D nanoporous copper-supported tin thin-film anode for LIBs by electroless plating a thin layer of tin onto sandwich-typed NPC (which serves as both the current collector and substrate of active materials). The unique 3D NPC is fabricated by partly chemical dealloying of as-cast Al 50 at.% Cu alloy slices in an acidic solution. The obtained 3D-NPC/Sn thin-film anode, as an active/inactive composite, could take advantage of nanoporous structure for better mass transport and accommodation of the mechanical strains during charge-discharge cycling. Thus, the better electrochemical performance can be obtained

in comparison with the 2D tin thin-film anode (2D-TTA) and the probable mechanism is discussed. This unique nano-architectured electrode exhibits a promising application in high-performance LIBs.

2. EXPERIMENTAL SECTION

2.1. Preparation and characterization of the sandwich-typed 3D NPC/Sn thin-film anode

Al-Cu alloy with nominal composition of 50 at.% Cu was prepared from pure Al (99.9 wt.%) and pure Cu (99.999 wt.%). Voltaic arc heating was employed to melt the charges in a copper crucible under an argon atmosphere, and then the melt was cooled down into ingots in situ. Subsequently, the alloy ingots were processed into slices by wire-cutting EDM with the thickness of about 300 μm. Prior to further treatment, the slices were washed and polished to remove oil and oxides formed on the surface. The dealloying of Al 50 at.% Cu alloy was performed in 5 wt.% HCl aqueous solution at 90℃ for different times. After dealloying, the samples were rinsed with distilled water and dehydrated alcohol for several times. The sandwich-typed 3D NPC slices were obtained after dried in a vacuum oven at 60℃ for 48 h. To prepare the 3D-NPC/Sn thin-film anode, electroless plating of tin was typically conducted in a plating bath containing 0.33M $SnSO_4$, 3.85M NaOH, 0.9M NaH_2PO_2 and 0.66M sodium citrate at 75℃ for 4 min. For comparison, 2D-TTA was also prepared by electroless plating tin onto 2D flat copper foil under the same conditions.

Microstructural characterization and analysis of the sandwich-typed NPC and 3D-NPC/Sn samples were made using X-ray diffraction (XRD, Rigaku D/Max-2400) with Cu Kα radiation, scanning electron microscopy (FESEM, Hitachi S-4800) with an energy dispersive X-ray (EDX) analyzer.

2.2. Cell assemble and electrochemical measurements

Electrochemical charge-discharge behaviors were investigated in simulant cells assembled with the as-prepared anode, lithium foil and Celgard 2300 membrane in an Ar-filled glove box (MB-10-G with TP170b/mono, MBRAUN). Electrolyte was 1M $LiPF_6$ in a mixed solution of EC and DEC (1:1 by v/v). Each cell was aged for 24 h at room temperature before commencing the electrochemical tests. The galvanostatic charge-discharge measurements were carried out in a battery test system (NEWARE BTS-610, Newware Technology Co., Ltd., China) for a cut-off potential of 0.01-1.5V (vs. Li/Li^+) at ambient temperature.

3. RESULTS AND DISCUSSION

Figure 1 shows the microstructure of as-dealloyed samples by chemical dealloying of as-cast Al 50 at.% Cu alloy slices in the 5 wt.% HCl solution at 90℃ for different times. For the products upon

dealloying for 3 h, a thin layer of non-uniform porous structure can be formed on the outmost surface of the initial Al-Cu alloy, indicating the evolution of porous structure is occurring at this stage.

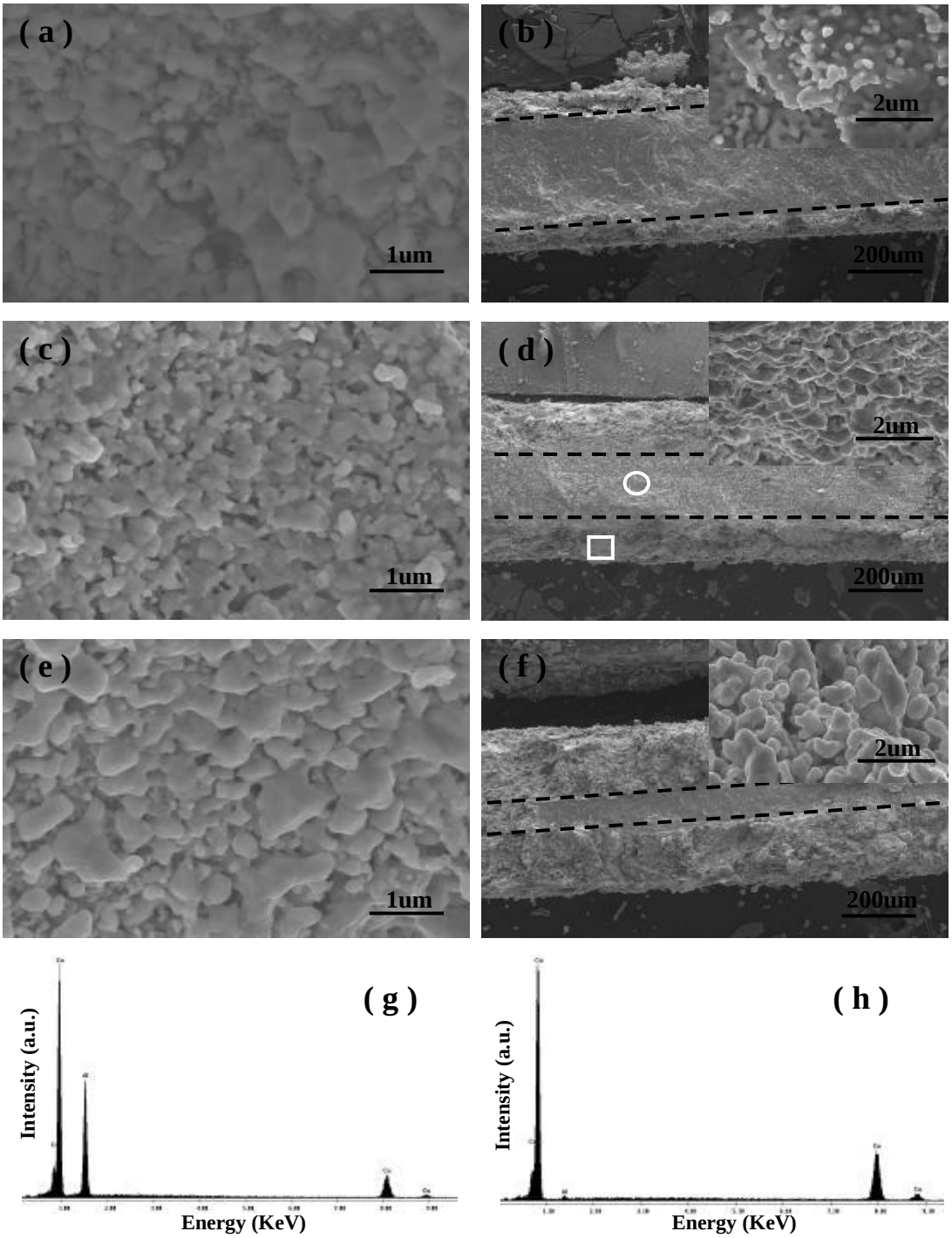

Figure 1. SEM images of as-dealloyed samples by chemical dealloying of as-cast Al 50 at.% Cu alloy slices in the 5 wt.% HCl solution at 90℃ for (a-b) 3 h, (c-d) 5 h, (e-f) 10 h. Parts a, c and e are the plane views; parts b, d and f are the section views, in which broken line denotes the boundary between porous structure and alloy layer. (g-h) EDX spectra of porous structure and alloy layer in samples marked by circle and square in part d. a.u.: arbitrary units.

When the dealloying time reaches 5 h, it is clear that the surface of as-dealloyed samples exhibits an open, 3D bicontinuous interpenetrating ligament-pore structure with relatively large ligament sizes of ~ 300 nm as compared with that of pore dimensions (~ 100 nm). Meanwhile, from the section-view image of samples, we note that the thickness of layer of porous structure is remarkably increased and a sandwich-typed microstructure composed of alternating porous structure layer and alloy layer (~ 1:1 by thickness) can be obtained.

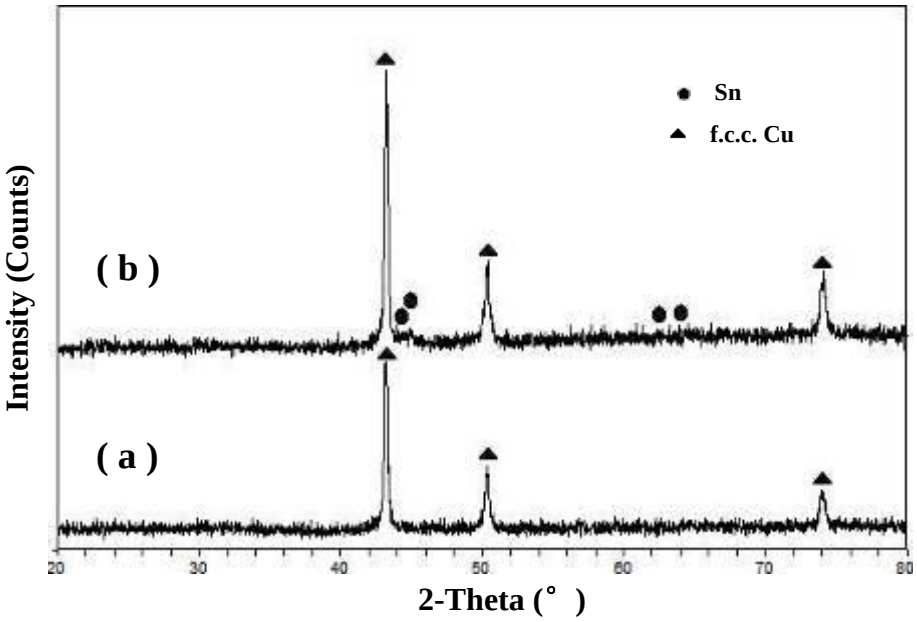

Figure 2. XRD patterns of (a) the 3D NPC current collector by chemical dealloying of Al 50 at.% Cu alloy slices in the 5 wt.% HCl solution at 90℃ for 5 h and (b) the 3D-NPC/Sn thin-film anode after electroless plating tin at 75℃ for 4 min.

With the dealloying time keeping increasing, the porous structure layer gradually coarsens due to the Ostwald ripening effects [55], which is markedly thicker than the central alloy layer as the dealloying time up to 10 h. EDX analysis has been performed on the sandwich-typed 3D NPC slices upon dealloying for 5 h, and typical spectra are shown in Figure 1g-h. It is obvious that the alloy layer is enriched in Al, and both atomic percentages of Al and Cu in the alloy layer are close to 50, while nearly all of Al is removed in the porous structure layer during dealloying. The present result demonstrates that the bilateral porous structure is Cu phase, and the central alloy is AlCu phase.

In order to take advantages of merits of the special 3D porous structure (such as large specific surface area and good electrical conductive network) and maintain its mechanical strength, the sandwich-typed 3D NPC slices upon dealloying in the 5wt.% HCl solution at 90℃ for 5 h were chosen as desirable current collectors and substrates of active materials herein. Figure 2 shows the XRD patterns of the 3D NPC current collector and the 3D-NPC/Sn thin-film anode upon electroless plating tin for 4 min, respectively. The filled circles and triangles stand for Sn and Cu, respectively. As can be seen from Figure 2a, only a face-centered cubic (f.c.c.) Cu phase can be identified in the 3D NPC

current collector under the X-ray detection limit. After electroless plating, the XRD result of the 3D-NPC/Sn thin-film anode indicates the presence of two basic phases: the minor deposited product tetragonal β-Sn and original f.c.c. Cu substrate. The result clearly demonstrates that the tin as active material has been successfully deposited onto the 3D NPC substrate upon electroless plating tin for 4 min.

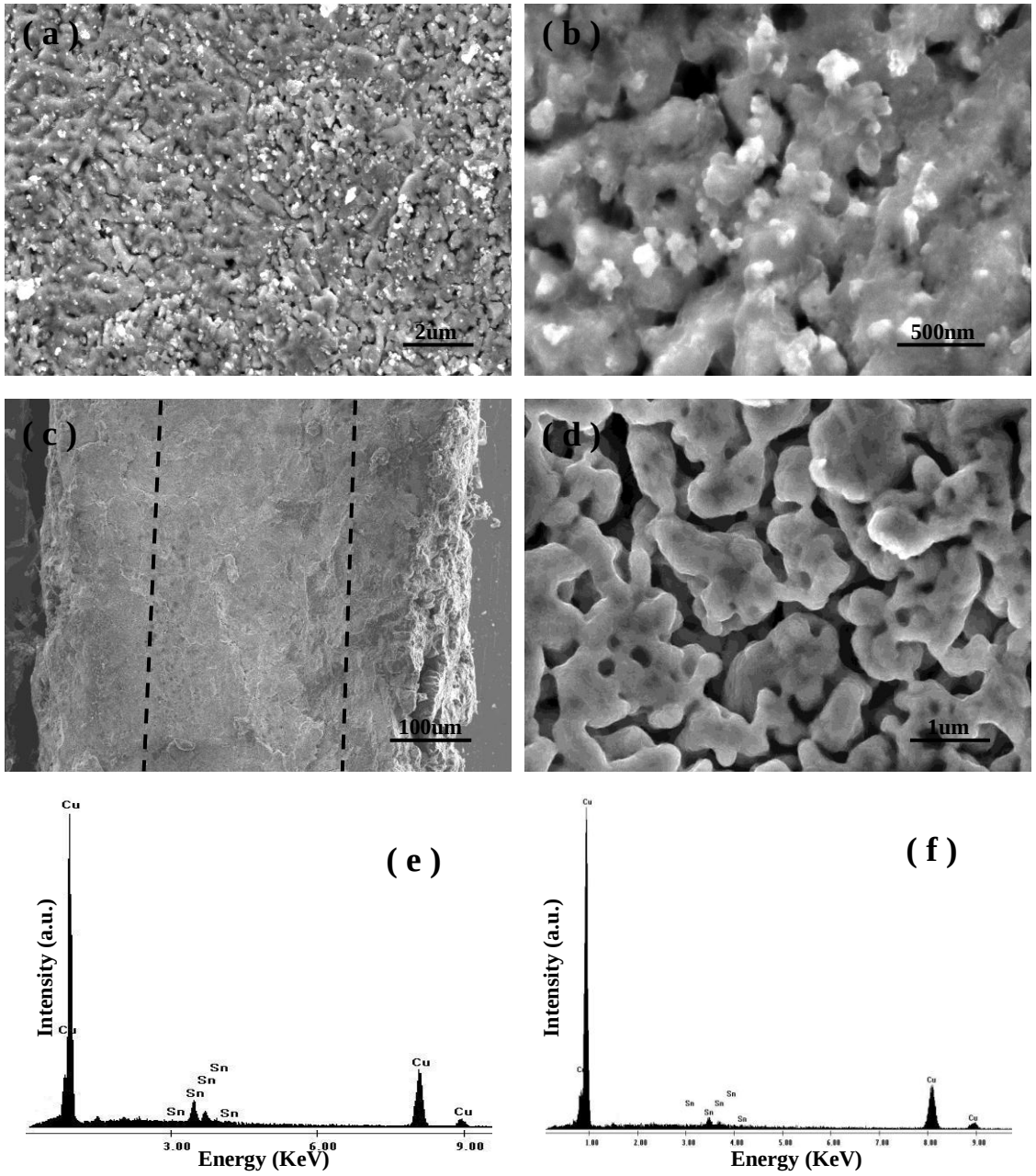

Figure 3. SEM images of sandwich-typed 3D NPC/Sn thin-film anode by electroless plating tin on the 3D NPC current collector in the alkaline solution at 75℃ for 4 min. Parts a and b are the plane views; parts c and d are the section views, in which broken line denotes the boundary between porous structure and alloy layer. (e-f) EDX spectra of porous structures corresponding to parts b and d. a.u.: arbitrary units.

Figure 3 shows the plane- and section-view SEM images of sandwich-typed 3D NPC/Sn thin-film anode by electroless plating tin on the 3D NPC current collector in the alkaline solution for 4 min. It is clear that a uniform and smooth layer of tin covers the surface and interior of porous structure of the 3D current collector, and the open, 3D bicontinuous interpenetrating porous network morphology with pore sizes of ~ 200 nm, which is slightly larger than before, can be well preserved in the resulting anode after electroless plating. Additionally, EDX analysis has been performed on the 3D NPC/Sn thin-film anode, and typical spectra are shown in Figure 3e-f. Obviously, both the surface and interior of the 3D porous electrode are enriched in Sn, confirming tin layer has been well deposited on the ligaments of the 3D porous substrate after electroless plating tin.

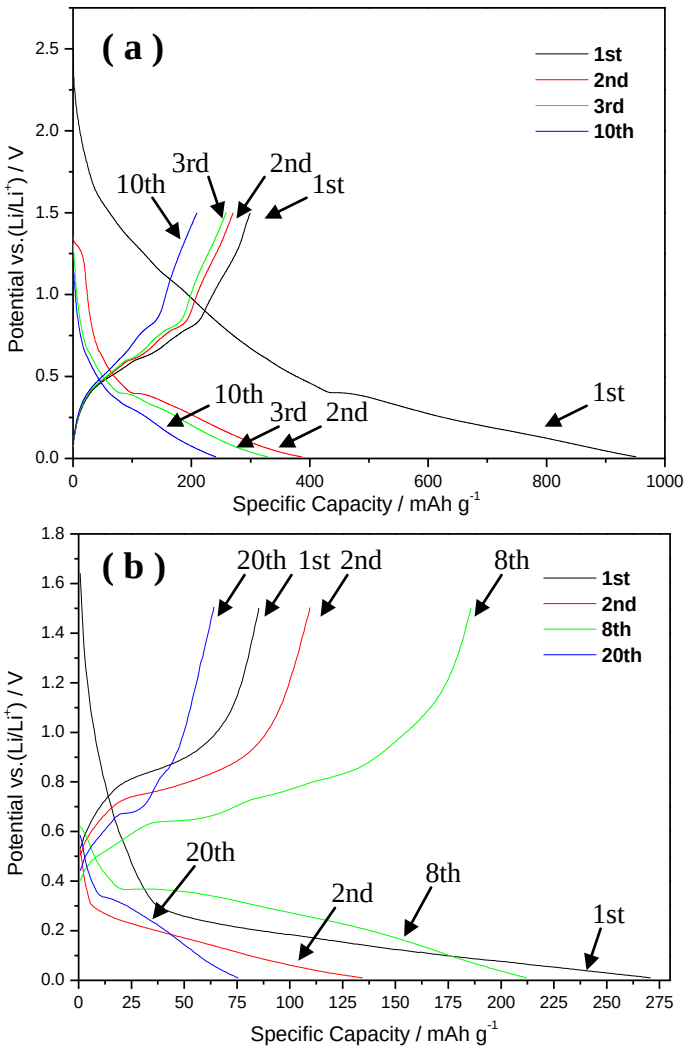

Figure 4. Charge-discharge curves of (a) the 3D-NPC/Sn thin film anode and (b) the 2D-TTA at 0.1C rate between 1.5V and 0.01V.

The charge-discharge curves of sandwich-typed 3D NPC/Sn thin-film anode at the 0.1C rate between 1.5V and 0.01V shown in Figure 4a suggest a poor efficiency during the first cycle with 964 mAh g^{-1} initial discharge capacity and 31% columbic efficiency. It is mainly assigned to the compact

microstructure of tin film which severely hinders the delithiation process and the formation of a solid electrolyte interphase (SEI) layer due to decomposition of electrolyte on the tin surface [56,57]. According to the first discharge of 3D thin-film anode, two plateaus around 0.2V and 0.5V can be clearly identified, which can be ascribed to lithium insertion into different Li_xSn phases [2,58]. During the charge, the 3D thin-film anode shows a slope ranging from 0.5V to 0.8V, corresponding to reversible delithiation from Li-Sn alloy. In the following cycles, charge-discharge curves have the similar profile with good cyclability and efficiency.

Figure 4b shows the charge-discharge curves of the 2D-TTA that tested at the 0.1C rate between 1.5V and 0.01V. The first discharge curve of 2D-TTA exhibits Li intercalation plateaus at around 0.2V, and the initial discharge capacity is just 270 mAh g^{-1}, about 1/4 of that of 3D NPC/Sn thin-film anode. In the following cycles, the reversible capacity rises first and then decreases sharply, reaching the peak value (185 mAh g^{-1}) at the eighth cycle. It is most likely related to the large exposure of active surface of tin caused by cracking during charge-discharge cycling [5]. During the 30th cycle, the reversible capacity only remains 39 mAh g^{-1}, which is ascribed to the serious pulverization and shedding of tin from the flat current collector [4-7,24]. As a result, the following charge/discharge capacity is even less than 14.4% of the first discharge capacity. Therefore, Compared to the 2D-TTA, the 3D NPC/Sn thin-film electrode possesses higher capacity and better capacity retention.

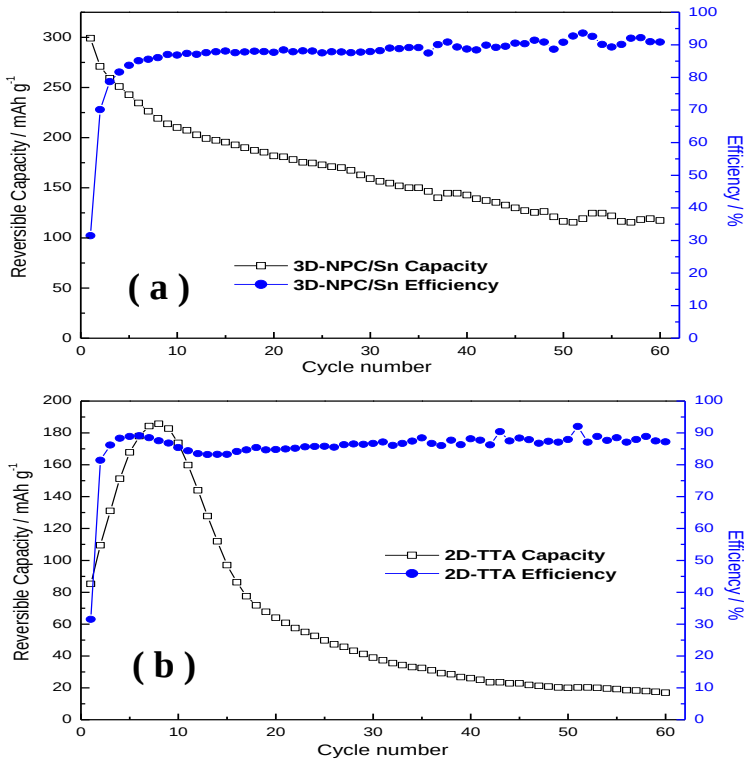

Figure 5. Cycle performances of (a) the 3D-NPC/Sn thin film anode and (b) the 2D-TTA at 0.1C rate.

Figure 5 shows the cycle performance of 3D NPC/Sn thin-film anode and 2D-TTA. Compared to the 2D-TTA, the improved cycle performance for the 3D NPC/Sn anode is exhibited in both higher capacity and better Coulombic efficiency. The charge capacity of 3D NPC/Sn thin-film anode in the

first cycle is 300 mAh g^{-1}, which is 3 times higher than that of 2D-TTA, and this ratio rises up to 7 times at the 60th cycle, higher than the reported nano-architectured electrodes [17]. Moreover, the reversible capacity retention of 3D thin-film anode remains 70% after 10 cycles, 61% after 20 cycles and still 40% after 60 cycles. It is worthwhile noting that considering the relatively high tin loading (tens of mg), the 3D NPC/Sn thin-film anode exhibits evidently better capacity retention than other batteries with similar tin film anode ever reported [7]. Except for the first several cycles, its Coulombic efficiency always maintains above 90%. In contrast, the reversible capacity retention of 2D-TTA only remains 20% after 60 cycles, and its Coulombic efficiency is rarely beyond 90%.

The good performance of the 3D NPC/Sn thin-film anode demonstrates the merits of the special 3D nanostructured electrode developed from dealloying, which contains uniform porous structure with relatively large pore sizes. On the one hand, the large-sized pores could facilitate the solvent diffusion and mass transportation, and increase effective surface area of electrode connecting with electrolyte. On the other hand, the 3D porous structure of electrode can also contribute greatly to enlarge the surface area and accommodate more tin with less thickness. The large specific surface area enables higher active area during reaction and thus brings better capacity. The small thickness of tin layer relieves the mechanical stress associated with huge volume expansion during cycling. Besides, the 3D nanoporous structure could hold tin particles in case of delaminating from current collector even when cracks and pulverization occurred inside porous structure.

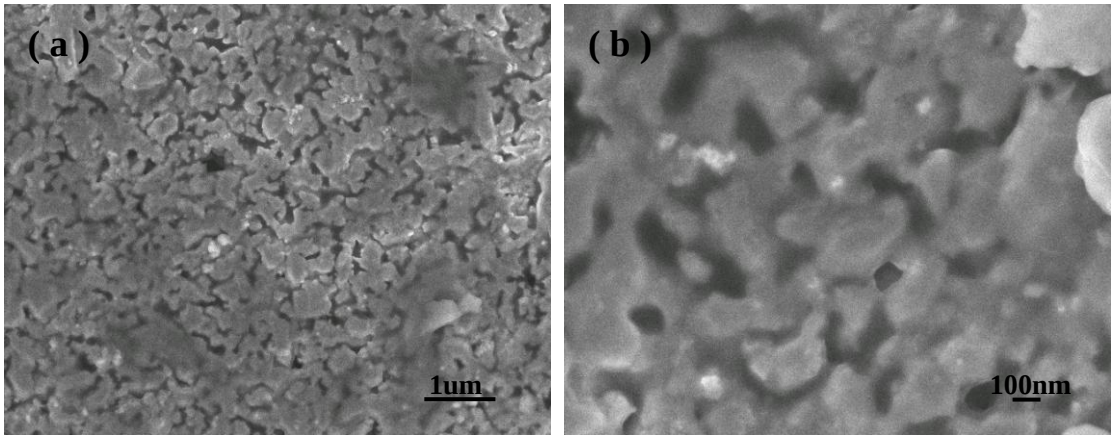

Figure 6. SEM images of the 3D-NPC/Sn thin film electrode after 60 cycles at 0.1C rate.

To further understand the failure mechanism of 3D NPC/Sn thin-film electrode, SEM micrographs of the 3D thin-film anode after 60 galvanostatical charge-discharge cycles were shown in Figure 6. It clearly shows that the 3D porous strcuture of the NPC/Sn thin-film electrode is not subjected to severe damage after 60 cyclic volume changes, indicating the sandwich-typed NPC substrate possesses good mechanical strength and can accommodate structural strain to some extent during lithiation/delithiation reactions. It should be noted that, however, the repeated lithiation/delithiation process still causes partial pulverization and shedding of tin from the surface of

the 3D electrode during cycling as shown in the high-magnification SEM image (Figure 6b), and thus leading to the gradual loss of capacity and fading of cycle performation.

Based on our present work, it is believable that one can employ this simple and effective strategy to obtain the sandwich-typed 3D nanoporous metal-supported tin thin-film anode with good mechanical strength and satisfactory electrochemical performance for LIBs. Moreover, it needs to be point out that the electrochemical performance of the 3D NPC/Sn thin-film electrode could be further improved by optimizing the deposition condition and developing the new coating approch of active materials, which will be our focuses in the future work.

4. CONCLUSION

In summary, a unique sandwich-typed three-dimensional nanoporous copper-supported tin thin-film anode has been prepared by partly chemical dealloying of as-cast Al 50 at.% Cu alloy slices followed by electroless depositing of a thin layer of tin in an alkaline solution. Its application in the lithium-ion battery demonstrates that the unique 3D nanoporous electrode with relatively large pore sizes can be a promising strategy to prepare high performance anode materials. The sandwich-typed 3D nanoporous copper with large surface area and good mechanical strength could work as both the current collector and substrate for active materials. Compared to the 2D-TTA, the 3D NPC/Sn thin film electrode with a relatively high tin loading exhibits higher capacity and better cycle performance, which can be ascribed to the special 3D porous structure and large active surface area. Additionally, optimizing the deposition condition of active materials, developing the new coating strategy of active materials and further improving the capacity fading may open the possibility to use this special microstructure for high-performance LIBs.

ACKNOWLEDGEMENT
We give thanks to financial support by the State Key Basic Research Program of PRC (2013CB934000, 2007CB936502), the National Natural Science Foundation of China (50574008, 50954005, 51074011), the National 863 Program Project (2008AA03Z208, 2011AA11A257), the China Postdoctoral Science Foundation Funded Project (2011M500214), the Basic Research Fund Project of Beihang University (501LJJC2012101001, 501LKGY2012101004), and the Shanghai Aerospace Science and Technology Innovation Fund Project (SAST201269). Also, we are grateful to Prof. T. Zhang and Dr. J.F. Wang for assistance in preparation of the Al-Cu alloy ingots.

References

1. M. Winter and R. J. Brodd, *Chem. Rev.*, 104 (2004) 4245.
2. M. Winter and J. O. Besenhard, *Electrochim. Acta*, 45 (1999) 31.
3. G. X.Wang, J. H. Ahn, J. Yao, S. Bewlay and H. K. Liu, *Electrochem. Commun.*, 6 (2004) 689.
4. K. D. Kepler, J. T. Vaughey and M. M. Thackeray, *J. Power Sources*, 81-82 (1999) 383.
5. A. H. Whitehead, J. M. Elliott and J. R. Owen, *J. Power Sources*, 81-82 (1999) 33.
6. J. Yang, M. Wachtler, M. Winter and J. O. Besenhard, *Electrochem. Solid-State Lett.*, 2 (1999) 161.

7. H. Li, X. J. Huang, L. Q. Chen, Z. G.Wu and Y. Liang, *Electrochem. Solid-State Lett.,* 2 (1999) 547.
8. Z. P. Guo, J. Z. Wang, H. K. Liu and S. X. Dou, *J. Power Sources,* 146 (2005) 448.
9. M. Valvo, U. Lafont, D. Munao and E. M. Kelder, *J. Power Sources,* 189 (2009) 297.
10. W. Choi, J. Y. Lee, B. H. Jung and H. S. Lim, *J. Power Sources,* 136 (2004) 154.
11. Y. Hu, Y. Guo, W. Sigle, S. Hore, P. Balaya and J. Maier, *Nat. Mater.,* 5 (2006) 713.
12. O. Mao, R. L. Turner, I. A. Courtney, B. D. Fredericksen, M. I. Buckett, L. J. Krause and J. R. Dahn, *Electrochem. Solid-State Lett.,* 2 (1999) 3.
13. A. Trifonova, M. Wachtler, M. R. Wagner, H. Schriettner, C. Mitterbauer, F. Hofer, K. C. Möller, M. Winter and J. O. Besenhard, *Solid State Ionics,* 168 (2004) 51.
14. T. Jiang, S. Zhang, X. Qiu,W. Zhu and L. Chen, *J. Power Sources,* 166 (2007) 503.
15. T. Jiang, S. Zhang, X. Qiu,W. Zhu and L. Chen, *Electrochem. Commun.,* 9 (2007) 930.
16. A. S. Aricò, P. Bruce, B. Scrosati and J. M. Tarascon, *Nat. Mater.,* 4 (2005) 366.
17. L. Bazin, S. Mitra, P. L. Taberna, M. Gressier, M. J. Menu, A. Barnabé, P. Simon and J. M. Tarascon, *J. Power Sources,* 188 (2009) 578.
18. S. H. Ju, H. C. Jang and Y. C. Kang, *J. Power Sources,* 189 (2009) 163.
19. W. Pu, X. He, J. Ren, C. Wan and C. Jiang, *Electrochim. Acta,* 50 (2005) 4140.
20. H. Guo, S. Zhao, H. Zhao and Y. Chen, *Electrochim. Acta,* 54 (2009) 4040.
21. P. A. Connor and J. T. S. Irvine, *Electrochim. Acta,* 47 (2002) 2885.
22. M. Martos, J. Morales and L. Sánchez, *Electrochim. Acta,* 46 (2000) 83.
23. G. X. Wang, J. Yao, H. K. Liu, S. X. Dou and J. Ahn, *Electrochim. Acta,* 50 (2004) 517.
24. N. Tamura, R. Ohshita, M. Fujimoto, S. Fujitani, M. Kamino and I. Yonezu, *J. Power Sources,* 107 (2002) 48.
25. C. Arbizzani, S. Beninati, M. Lazzari and M. Mastragostino, *J. Power Sources,* 141 (2005) 149.
26. M. Yoshio, T. Tsumura and N. Dimov, *J. Power Sources,* 146 (2005) 10.
27. J. Y. Xiang, J. P. Tu, X. L.Wang, X. H. Huang, Y. F. Yuan, X. H. Xia and Z. Y. Zeng, *J. Power Sources,* 185 (2008) 519.
28. L. Huang, H. B.Wei, F. S. Ke, X. Y. Fan, J. T. Li and S. G. Sun, *Electrochim. Acta,* 54 (2009) 2693.
29. G. J. Davies and S. Zhen, *J. Mater. Sci.,* 18 (1983) 1899.
30. G. C. Bond and D. T. Thompson, *Catal. Rev.,* 41 (1999) 319.
31. T. You, O. Niwa, M. Tomita and S. Hirono, *Anal. Chem.,* 75 (2003) 2080.
32. J. R. Weissmueller, N. Viswanath, D. Kramer, P. Zimmer, R. Wuerschum and H. Gleiter, *Science,* 300 (2003) 312.
33. S. H. Joo, S. J. Choi, K. J. Kwa and Z. Liu, *Nature,* 412 (2001) 169.
34. J. Erlebacher, M. J. Aziz, A. Karma, N. Dimitrov and K. Sieradzki, *Nature,* 410 (2001) 450.
35. W. B. Liu, S. C. Zhang, N. Li, J. W. Zheng and Y. L. Xing, *J. Electrochem. Soc.*, 157 (2010) D666.
36. Z. H. Zhang, Y. Wang, Y. Z. Wang, X. G. Wang, Z. Qi, H. Ji and C. C. Zhao, *Scripta Mater.,* 62 (2010) 137.
37. W. B. Liu, S. C. Zhang, N. Li, J. W. Zheng and Y. L. Xing, *Corrosion Sci.,* 53 (2011) 809.
38. Z. Qi, C. C. Zhao, X. G. Wang, J. K. Lin, W. Shao, Z. H. Zhang and X. F. Bian, *J. Phys. Chem. C,* 113 (2009) 6694.
39. W. B. Liu, S. C. Zhang, N. Li, J. W. Zheng and Y. L. Xing, *Microporous Mesoporous Mater.,* 138 (2011) 1.
40. Z. H. Zhang, Y. Wang, Z. Qi, J. K. Lin and X. F. Bian, *J. Phys. Chem. C,* 113 (2009) 1308.
41. W. B. Liu, S. C. Zhang, N. Li, J. W. Zheng, S. S. An and Y. L. Xing, *Int. J. Electrochem. Sci.,* 7 (2012) 6365.
42. W. B. Liu, S. C. Zhang, N. Li, J. W. Zheng, S. S. An and Y. L. Xing, *Int. J. Electrochem. Sci.,* 7 (2012) 2240.
43. Y. Ding and J. Erlebacher, *J. Am. Chem. Soc.,* 125 (2003) 7772.

44. W. B. Liu, S. C. Zhang, N. Li, J. W. Zheng, S. S. An and Y. L. Xing, *Corrosion Sci.*, 58 (2012) 133.
45. Y. Ding, Y. J. Kim and J. Erlebacher, *Adv. Mater.*, 16 (2004) 1897.
46. W. B. Liu, S. C. Zhang, N. Li, J. W. Zheng and Y. L. Xing, *Int. J. Electrochem. Sci.*, 6 (2011) 5445.
47. W. B. Liu, S. C. Zhang, N. Li, J. W. Zheng, S. S. An and G. X. Li, *Int. J. Electrochem. Sci.*, 7 (2012) 7993.
48. L. H. Qian and M. W. Chen, *Appl. Phys. Lett.*, 91 (2007) 083105.
49. W. B. Liu, S. C. Zhang, N. Li, J. W. Zheng and Y. L. Xing, *J. Electrochem. Soc.*, 158 (2011) D611.
50. Y. Ding, A. Mathur, M. W. Chen and J. Erlebacher, *Angew. Chem., Int. Ed.*, 44 (2005) 4002.
51. W. B. Liu, S. C. Zhang, N. Li, S. S. An and J. W. Zheng, *Int. J. Electrochem. Sci.*, 7 (2012) 9707.
52. W. B. Liu, S. C. Zhang, N. Li, J. W. Zheng and Y. L. Xing, *J. Electrochem. Soc.*, 158 (2011) D91.
53. J. Erlebacher, *J. Electrochem. Soc.*, 151 (2004) C614.
54. W. B. Liu, S. C. Zhang, N. Li, J. W. Zheng and Y. L. Xing, *J. Mater. Sci. Technol.*, 28 (2012) 693.
55. A. M. Hodge, J. Biener, J. R. Hayes, P. M. Bythrow, C. A. Volkert and A. V. Hamza, *Acta Mater.*, 55 (2007) 1343.
56. M. Inaba, T. Uno and A. Tasaka, *J. Power Sources*, 146 (2005) 473.
57. S. D. Beattie, T. Hatchard, A. Bonakdarpour, K. C. Hewitt and J. R. Dahn, *J. Electrochem. Soc.*, 150 (2003) A701.
58. R. A. Huggins, *J. Power Sources*, 13 (1999) 81.